AD-A065 588 OHIO STATE UNIV COLUMBUS ELECTROSCIENCE LAB F/G 20/14
AN ASYMPTOTIC RESULT FOR THE SCATTERING OF A PLANE WAVE BY A SM--ETC(U)
MAR 78 P H PATHAK N62269-76-C-0554
UNCLASSIFIED ESL-784583-3 NADC-79043-30 NL

| OF |
AD
AO 65588

END
DATE FILMED
5--79
DDC

AN ASYMPTOTIC RESULT FOR THE SCATTERING OF A PLANE WAVE BY A SMOOTH CONVEX CYLINDER

P. H. Pathak

Technical Report 784583-3

Contract No. N62269-76-C-0554

March 1978

Department of the Navy
Naval Air Development Center
Warminster, Pennsylvania 18974

UNCLASSIFIED

SECURITY CLASSIFICATION OF THIS PAGE *(When Data Entered)*

REPORT DOCUMENTATION PAGE		READ INSTRUCTIONS BEFORE COMPLETING FORM
1. REPORT NUMBER NADC-79043-30	2. GOVT ACCESSION NO.	3. RECIPIENT'S CATALOG NUMBER
4. TITLE *(and Subtitle)* AN ASYMPTOTIC RESULT FOR THE SCATTERING OF A PLANE WAVE BY A SMOOTH CONVEX CYLINDER		5. TYPE OF REPORT & PERIOD COVERED Technical Report 6. PERFORMING ORG. REPORT NUMBER ESL 784583-3
7. AUTHOR(s) P. H. Pathak		8. CONTRACT OR GRANT NUMBER(s) Contract N62269-76-C-0554
9. PERFORMING ORGANIZATION NAME AND ADDRESS The Ohio State University ElectroScience Laboratory, Department of Electrical Engineering, Columbus, Ohio 43212		10. PROGRAM ELEMENT, PROJECT, TASK AREA & WORK UNIT NUMBERS 63206N, WR6-1154 WTW180000, RA702
11. CONTROLLING OFFICE NAME AND ADDRESS Department of the Navy Naval Air Development Center Warminster, Pennsylvania 18974		12. REPORT DATE March 1978 13. NUMBER OF PAGES 37
14. MONITORING AGENCY NAME & ADDRESS(if different from Controlling Office)		15. SECURITY CLASS. *(of this report)* Unclassified 15a. DECLASSIFICATION/DOWNGRADING SCHEDULE

16. DISTRIBUTION STATEMENT *(of this Report)*

Approved for public release;distribution unlimited

17. DISTRIBUTION STATEMENT *(of the abstract entered in Block 20, if different from Report)*

18. SUPPLEMENTARY NOTES

19. KEY WORDS *(Continue on reverse side if necessary and identify by block number)*

Smooth convex cylinder
Electromagnetic scattering
Geometrical theory of diffraction (GTD)
Transition region
Uniform asymptotic result
Off-fuselage aircraft antennas

20. ABSTRACT *(Continue on reverse side if necessary and identify by block number)*

An approximate asymptotic high frequency result which is convenient for engineering applications is obtained for the field scattered by a smooth, perfectly-conducting convex cylinder when it is illuminated by a plane wave. This result is uniform in the sense that it remains valid within the transition regions adjacent to the shadow boundaries where the pure ray optic (or GTD) solution fails, and it automatically

DD FORM 1 JAN 73 1473 EDITION OF 1 NOV 65 IS OBSOLETE

UNCLASSIFIED

SECURITY CLASSIFICATION OF THIS PAGE *(When Data Entered)*

20.

reduces to the ray optic solution exterior to the transition regions where the latter solution becomes valid. Furthermore, this result is expressed in the convenient format of the GTD, and it employs the same ray paths as in the GTD solution. This uniform result is not valid in the close neighborhood of the cylinder; hence, a separate asymptotic result is presented for this special case in a form which is also convenient for applications. The asymptotic results presented here are useful for predicting the patterns of antennas radiating in the presence of convex, conducting cylindrical structures.

CONTENTS

I. INTRODUCTION

The geometrical theory of diffraction (GTD) [Keller,1953,1956,1962] provides a very convenient and accurate method for analyzing the problem of high frequency plane wave scattering by smooth convex surfaces except in the vicinity of the shadow boundaries and caustics. Thus, approximate asymptotic high frequency results which remain valid even within the regions where the GTD fails are developed in this paper for the case of a smooth, convex cylinder illuminated by a plane wave. This work is motivated by the need to analyze the radiation patterns of antennas mounted near curved surfaces such as an aircraft fuselage [Burnside,1972, Burnside, et al.,1975] or a ship mast.

In the GTD analysis of the scattering of waves by an impenetrable, smooth convex cylinder [Keller,1956], the total exterior field is associated with the usual incident and reflected rays of geometrical optics, together with the surface diffracted rays introduced by Keller. The geometric optical rays do not penetrate the convex body, and hence their field is zero within the shadow region. The surface diffracted rays are launched by the incident ray which grazes the surface as shown in Figure 1; these surface rays propagate into the shadow region and entirely account for the field therein. In that pure ray optical analyses fail at and near shadow boundaries, the GTD solution is valid in regions I and III as shown in Figure 1. It fails in the penumbral or transition region adjacent to the shadow boundary (SB) which is indicated as region II in Figure 1. The angular extent of this transition region is of the order $(2/k\rho_g(Q_1))^{1/3}$ where k refers to the wavenumber of the surrounding medium which is assumed here to be free space, and $\rho_g(Q_1)$ is the radius of curvature of the cylinder at the point of grazing incidence, i.e., at Q_1. GTD also fails in regions IV, V, and VI shown in Figure 1 which are usually referred to as the surface or caustic boundary layer regions. Regions IV and V are close to the surface of the obstacle which is a caustic of the surface diffracted rays; whereas, region VI is in the neighborhood of Q_1 which is a caustic of the reflected ray for grazing incidence. An asymptotic evaluation of the field within the shadow boundary transition regions, the surface boundary layer regions and also their common regions of overlap, is complicated by the fact that the field must change rapidly but smoothly from one form to another across these regions.

The problem of estimating the fields within the transition regions associated with the diffraction of waves by smooth, convex surfaces has received much attention, especially in connection with the theory of radio wave propagation around the earth. Fock made significant contributions to this area by developing a general asymptotic theory for the diffraction of waves by large convex surfaces [Fock,1957]. Fock expressed his general solution to this problem in terms of a canonical integral. In particular, Fock considered the Fresnel diffraction by a sphere [Fock,1951] in which he approximated the canonical integral asymptotically within the transition region; as a result, he was able

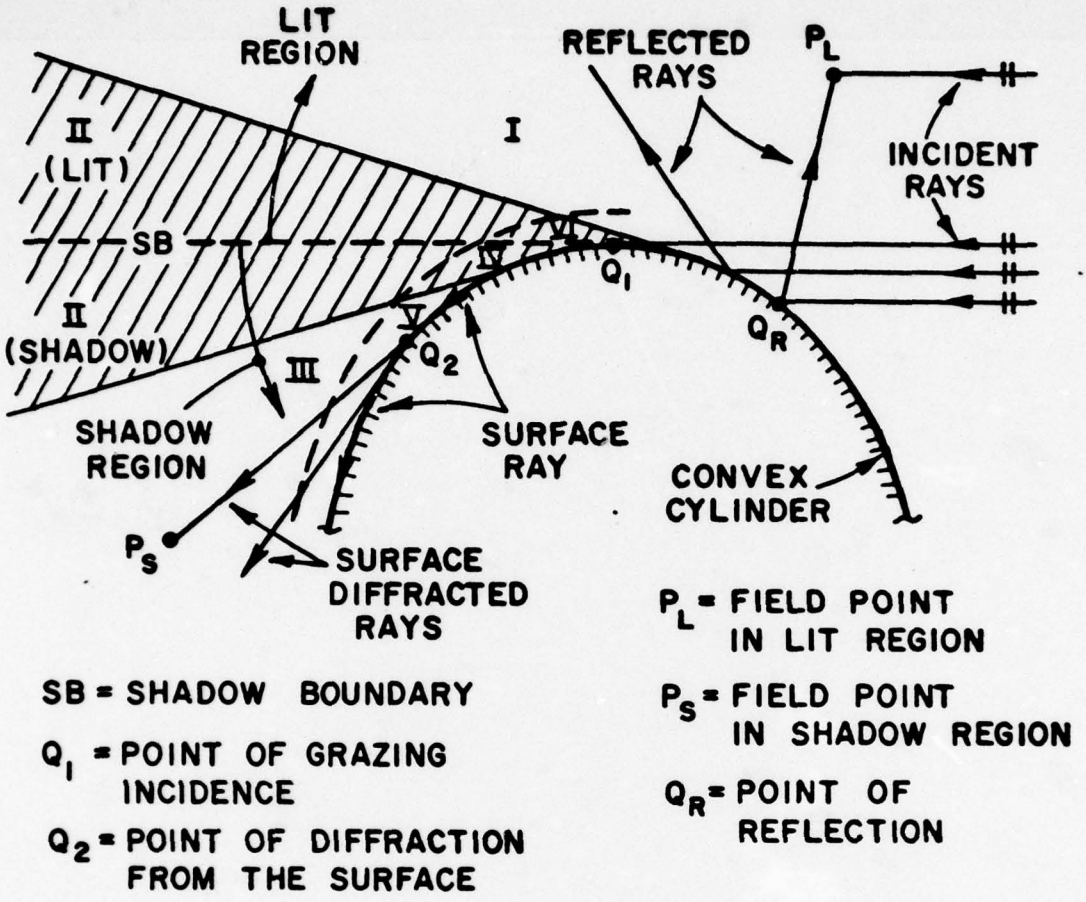

Figure 1. Rays associated with the plane wave scattering by a smooth convex cylinder.

to obtain a simpler solution in terms of tabulated, universal functions of a single parameter. That result [Fock,1951] is valid for heights of the source and observation points above the sphere which are small compared to the sphere radius. In another important paper on this subject by Wait and Conda [1959], this condition was relaxed so that the source and the observer could now be far from the diffracting surface. The results in [Wait and Conda,1959] are in terms of functions similar to those in [Fock,1951], but they are obtained from an asymptotic analysis of the canonical problem of the diffraction of a plane wave by a circular cylinder. However, the results in [Fock,1951] and [Wait and Conda,1959] do not reduce uniformly to the usual GTD ray solutions for the lit and shadow regions far from the shadow boundaries. Consequently,

one has to be concerned about the blending of the transition field and the ray optical field solutions. On the other hand, Logan and Yee [1962] were able to obtain an approximate uniform solution which recovers the GTD solution, by re-defining the parameters in Fock's canonical integral via an ad hoc procedure; whereas, Ivanov [1971] obtained a uniform result also in terms of Fock's canonical integral which recovers the GTD solution, by employing a coordinate transformation different from that of Fock. However, both of those uniform solutions are far too complex for numerical computations in the entire transition region. It is noted that the results in [Fock,1951] and [Wait and Conda,1959] are valid in region II which excludes regions IV and V of Figure 1. An extensive bibliography on other work dealing with various aspects of this diffraction problem may be found in [Logan and Yee,1962; Logan,1959], and [Borovikov and Kinber,1974].

In this paper, the canonical problem of plane wave scattering by a perfectly conducting circular cylinder is solved in a manner analogous to that in [Fock,1951], and some asymptotic approximations are introduced heuristically to obtain a uniform result for the total field which is valid within the transition region outside the surface boundary layer, and which automatically recovers the usual GTD or ray optical field solution exterior to this transition region. Hence, the present solution need not be introduced separately within the transition region, as a correction to the GTD solution. Furthermore, the present asymptotic result is expressed in the convenient format of the GTD; and it allows a simple interpretation in terms of the GTD rays. Only the leading terms in the asymptotic approximation are retained in this analysis. This uniform result is expressed in terms of tabulated, universal functions which are similar to those occurring in [Fock,1951] and [Wait and Conda,1959]; hence, the present result is very convenient for engineering applications. The analytical details pertaining to the solution of the canonical problem are presented in section II; these results are generalized to the convex cylinder case in section III. Since the uniform result presented here is not valid in the close vicinity of the surface and the surface boundary layer, a separate, approximate representation for the field which is valid very close to and on the surface is obtained in section IV. Numerical results are presented in section V to indicate the accuracy of the asymptotic results developed in sections III and IV.

II. DEVELOPMENT OF A UNIFORM RESULT FOR THE CIRCULAR CYLINDER CASE

An asymptotic high frequency analysis of the canonical problem of electromagnetic plane wave scattering by a perfectly conducting circular cylinder in free space is presented in this section. This analysis leads to a uniform asymptotic result for the field in the shadow boundary transition region which does not include the close vicinity of the cylinder. The geometry of this problem is illustrated in Figure 2. Since the problem is two-dimensional, it reduces to a scalar problem. It is assumed in the analysis that the field satisfies an $e^{j\omega t}$ time dependence which is suppressed. The total field exterior to the cylinder is denoted by u^T. Thus, $u^T = u^i + u^s$, where u^i denotes the incident field, and u^s denotes the field scattered by the cylinder.

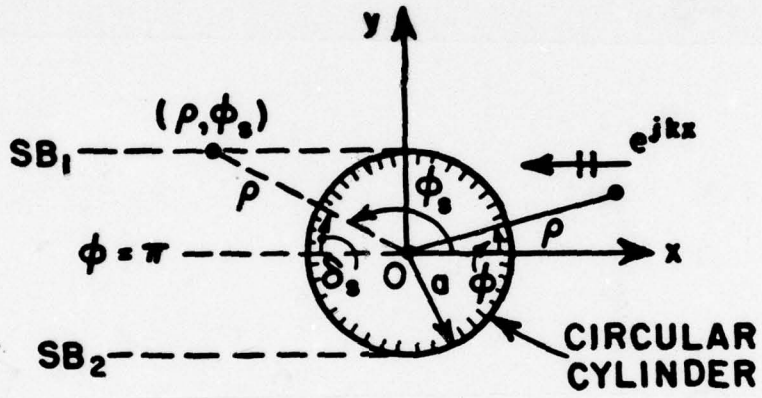

Figure 2. Geometry of the canonical problem.

If the incident electric field has only a z component, then the problem is of the TM_z (or acoustic soft) type. If the incident magnetic field has only a z component, then the problem is of the TE_z (or acoustic hard) type. Let

$$u^i = e^{jkx} = e^{jk\rho\cos\phi} \quad . \tag{1}$$

u^T satisfies the reduced wave equation and the following boundary conditions.

$$(\nabla_t^2 + k^2)\, u^T = 0; \quad \nabla_t^2 = \text{two dimensional Laplacian operator.} \tag{2}$$

$$Q\, u^T(\rho,\phi)\big|_{\rho=a} = 0 \; ; \quad Q = \begin{cases} 1 & \text{for } TM_z \text{ case.} \\ \dfrac{\partial}{\partial\rho} & \text{for } TE_z \text{ case.} \end{cases} \tag{3}$$

u^s satisfies the Sommerfeld radiation condition as $\rho \to \infty$. (4)

It is noted that u^i and u^s satisfy the reduced wave equation. A formal integral solution to (2) subject to (3) and (4) is given in [Bowman et.al.,1969] as

$$u^T = u + u^{cw} , \tag{5a}$$

where

$$u = \int_{-\infty - j\varepsilon}^{\infty - j\varepsilon} d\nu \left[J_\nu(k\rho) - \frac{QJ_\nu(ka)}{QH_\nu^{(2)}(ka)} H_\nu^{(2)}(k\rho) \right] e^{-j\nu\psi} \tag{5b}$$

or

$$u = \frac{1}{2} \int_{-\infty - j\varepsilon}^{\infty - j\varepsilon} d\nu \left[H_\nu^{(1)}(k\rho) - \frac{QH_\nu^{(1)}(ka)}{QH_\nu^{(2)}(ka)} H_\nu^{(2)}(k\rho) \right] e^{-j\nu\psi} \tag{5c}$$

with ε being a positive number, however small and

$$\psi = |\phi| - \frac{\pi}{2} , \quad \text{with } |\phi| < \pi \text{ (or } |\psi| < \frac{\pi}{2}). \tag{5d}$$

The term u^{cw} in (5a) represents the higher order diffraction effects which become negligible for large ka; more will be said about this term later in the analysis. Within the transition region, $\nu \sim 0$ (ka) such that one may employ the transformation

$$\nu = ka + m\tau \quad ; \quad m \equiv \left(\frac{ka}{2}\right)^{1/3} , \tag{6a;6b}$$

and replace $J_\nu(ka)$ and $H_\nu^{(1)}_{(2)}(ka)$ in (5b;5c) in the transition regions by

$$J_\nu(ka) \approx (m\sqrt{\pi})^{-1} V(\tau); \quad H_\nu^{(1)}_{(2)}(ka) \approx \mp j(m\sqrt{\pi})^{-1} w_{\frac{1}{2}}(\tau), \tag{7a;7b}$$

where the Airy functions $V(\tau)$ and $w_{\frac{1}{2}}(\tau)$ are defined as [Logan and Yee,1962]

$$2j\, V(\tau) = w_{\frac{1}{2}}(\tau) - w_2(\tau); \quad w_{\frac{1}{2}}(\tau) = \frac{1}{\sqrt{\pi}} \int_{\Gamma_{\frac{1}{2}}} dt\, e^{\tau t - t^3/3} . \tag{7c;7d}$$

The approximation in (7) is valid for large ka and $\nu \sim O(ka)$. It is assumed here that ka is large. The contour Γ_1 runs from $\infty e^{-j(2\pi/3)}$ to $\infty - j\varepsilon$, and Γ_2 is the complex conjugate of Γ_1. In (7), terms of $O(1/m^2)$ and higher are neglected. Therefore, within the transition regions (5b;5c) become via (7a;7b;7c and 7d):

$$u \approx m \int_{-\infty-j\varepsilon}^{\infty-j\varepsilon} d\tau [J_{\nu(\tau)}(k\rho) + j \frac{\partial V(\tau)}{\partial w_2(\tau)} H^{(2)}_{\nu(\tau)}(k\rho)] e^{-j(ka+m\tau)\psi} \tag{8a}$$

or

$$u \approx \frac{m}{2} \int_{-\infty-j\varepsilon}^{\infty-j\varepsilon} d\tau [H^{(1)}_{\nu(\tau)}(k\rho) + \frac{\partial w_1(\tau)}{\partial w_2(\tau)} H^{(2)}_{\nu(\tau)}(k\rho)] e^{-j(ka+m\tau)\psi} , \tag{8b}$$

with

$$\partial = \begin{cases} 1 , & \text{for the } TM_z \text{ case} \\ -m^{-1} \frac{\partial}{\partial \tau} , & \text{for the } TE_z \text{ case} \end{cases} . \tag{8c}$$

The field u may be initially decomposed as in [Fock,1951] for the sphere problem; namely, u is expressed as the sum of the integral in (8a) over the contour c_2 from $0-j\varepsilon$ to $\infty-j\varepsilon$, and the integral in (8b) over the contour c_1 from $-\infty-j\varepsilon$ to $0-j\varepsilon$, respectively. After rearrangement of terms, and the use of $H^{(1)}_{\nu(\tau)}(k\rho) = 2J_{\nu(\tau)}(k\rho) - H^{(2)}_{\nu(\tau)}(k\rho)$ in the integral over c_2, one obtains,

$$u = I_1 + I_2, \tag{9a}$$

where

$$I_1 = m \int_{c_1+c_2} d\tau \, J_{\nu(\tau)}(k\rho) e^{-j\nu(\tau)\psi} - \frac{m}{2} \int_{c_1} d\tau \, H^{(2)}_{\nu(\tau)}(k\rho) e^{-j\nu(\tau)\psi}, \tag{9b}$$

and

$$I_2 = jm \int_{c_2} d\tau \frac{\partial V(\tau)}{\partial w_2(\tau)} H^{(2)}_{\nu(\tau)}(k\rho) e^{-j\nu(\tau)\psi} + \frac{m}{2} \int_{c_1} d\tau \frac{\partial w_1(\tau)}{\partial w_2(\tau)} H^{(2)}_{\nu(\tau)}(k\rho) e^{-j\nu(\tau)\psi}. \tag{9c}$$

It is noted that I_1 is completely independent of the electrical properties of the cylinder. One may approximate the first integral asymptotically in (9b) via the method of steepest descent; it is seen that this term constitutes the incident field.

$$m \int_{c_1+c_2} d\tau\, J_{\nu(\tau)}(k\rho)e^{-j\nu(\tau)\psi} = \int_{-\infty-j\varepsilon}^{\infty-j\varepsilon} d\nu\, \frac{H_\nu^{(1)}(k\rho)+H_\nu^{(2)}(k\rho)}{2} e^{-j\nu\psi}$$

$$\sim e^{-jk\rho\sin\psi} = e^{jk\rho\cos|\phi|}; \quad |\phi|<\pi. \qquad (10)$$

The Hankel functions in the integrand of (10) are replaced by their Debye approximations prior to the asymptotic evaluation of the integral. The Debye approximation is [Bowman et. al.,1969]

$$H_\nu^{(1)}_{(2)}(k\rho) \sim \sqrt{\frac{2}{\pi k\rho\, \sin\gamma}}\, e^{\pm jk\rho\, \sin\gamma \mp j\nu\gamma \mp j\frac{\pi}{4}}; \quad \nu=k\rho\, \cos\gamma\ ; \quad 0<\mathrm{Re}\gamma<\pi\ . \qquad (11)$$

Since $0<\mathrm{Re}\gamma<\pi$ in (11), the $H_\nu^{(1)}(k\rho)$ term in (10) yields u^i for $0<|\phi|<\pi/2$ from the saddle point at $\gamma=\pi/2-|\phi|$, and contributes negligibly elsewhere; likewise, the $H_\nu^{(2)}(k\rho)$ term yields u^i for $\pi/2<|\phi|<\pi$ from the saddle point at $\gamma = |\phi|-\pi/2$. The remaining integrals in (9b) and (9c) will next be approximated asymptotically for the shadowed portion of the transition region in part A of this section; a corresponding development for the lit portion of the transition region will follow in part B. In the subsequent analysis, ϕ will be restricted to $0<\phi<\pi$ for convenience; the results for $-\pi<\phi<0$ may be readily obtained via symmetry.

A. Field Analysis for the Shadowed Transition Region

One may rewrite (9b) by incorporating (10) and by replacing $H_{\nu(\tau)}^{(2)}(k\rho)$ in the integral over c_1 with its integral representation,

$$H_{\nu(\tau)}^{(2)}(k\rho) = \frac{1}{\pi} \int_{c_B} d\beta\, e^{-jk\rho\sin\beta+j\nu(\tau)\beta}$$

to obtain

$$I_1 \approx e^{jk\rho\cos|\phi|} + \frac{e^{-jka\psi}}{2\pi j} \int_{C_B} d\beta \, \frac{e^{-jk\rho[\sin\beta - \frac{a}{\rho}\beta]}}{\psi-\beta}, \qquad (12)$$

where c_B is shown in Figure 3. The integrand in (12) possesses a saddle point at $\beta=\beta_s=\cos^{-1} a/\rho$, and a pole at $\beta = \beta_p = \psi$. For fixed values of ρ and a, β_s is a constant which is alternatively given by $\beta_s = \phi_s - \pi/2$, where ϕ_s is the value of ϕ at the shadow boundary (SB_1) as shown in Figure 2. The angular extent of the shadow zone (for $0<\phi<\pi$) is $\phi_s<\phi<\pi$; thus, $\beta_p>\beta_s$ and $\theta>0$ in the shadow region, where

$$\theta = \psi - \beta_s = \beta_p - \beta_s = \phi - \phi_s. \qquad (13)$$

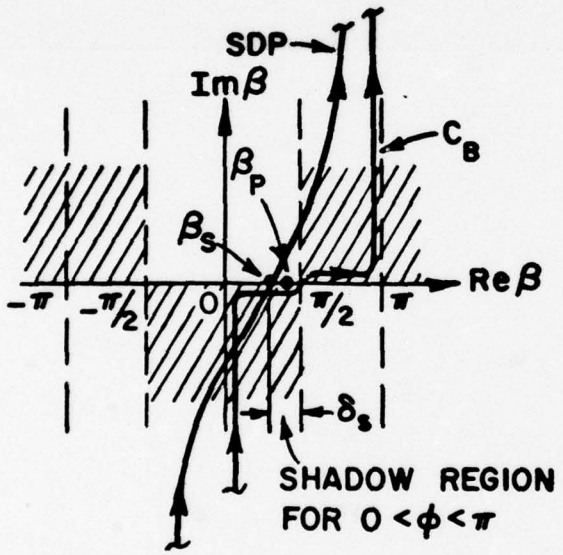

Figure 3. Location of β_s, β_p and SDP for the shadow region analysis.

The shaded areas in Figure 3 denote the regions where $e^{-jk\rho[\sin\beta - \frac{a}{\rho}\beta]}$ in (12) becomes vanishingly small for $|\mathrm{Im}\beta| \to \infty$; thus, one may deform the path c_B in (12) into the steepest descent path (SDP) through β_s as indicated in Figure 3. Since $\beta_s<\beta_p$ in the shadow, the pole at β_p is crossed in this contour deformation; therefore, it's residue given by $-e^{jk\rho\cos\phi}H(\phi-\phi_s)$ must be included in the evaluation of the integral. $H(\Delta)$ is a step function which is unity when $\Delta>0$, and zero when $\Delta<0$. Next, the exponent in the integrand of (12) may be approximated by it's three term Taylor expansion about $\beta=\beta_s$ for large $k\rho \sin\beta_s$ to obtain

$$I_1 \approx e^{jk\rho\cos\phi} - e^{jk\rho\cos\phi}\, H(\phi-\phi_s) - \frac{e^{-jk(s+a\theta)}}{2\pi j} \int_{SDP} d\beta\, \frac{e^{j\frac{ks}{2}(\beta-\beta_s)^2}}{\beta-\beta_p} \tag{14}$$

where

$$s^2 = \rho^2 - a^2 \; ; \qquad \rho \sin\beta_s = s. \tag{15a;15b}$$

Note that the first two terms in (14) cancel in the shadow region. This leaves the integral over the SDP which may be directly expressed in terms of the well tabulated Fresnel integral after employing the transformation

$$\mu = e^{-j\frac{\pi}{4}} (\beta-\beta_s)/\sqrt{2} \tag{16a}$$

which maps the SDP onto the real μ-axis ($-\infty<\mu<\infty$). Thus, for $\phi>\phi_s$

$$I_1 \approx - \frac{e^{-jk(s+a\theta)}}{2\pi j} \int_{-\infty}^{\infty} d\mu\, \frac{e^{-ks\mu^2}}{\mu-\mu_p} = \frac{e^{-j\frac{\pi}{4} - jka\theta}}{\sqrt{2\pi k}\,\theta} F[kL\tilde{a}]\, \frac{e^{-jks}}{\sqrt{s}}, \tag{16b}$$

where μ_p is the value of μ when $\beta=\beta_p$, and

$$F[kL\tilde{a}] = 2j\,|\sqrt{kL\tilde{a}}|\; e^{jkL\tilde{a}} \int_{|\sqrt{kL\tilde{a}}|}^{\infty} d\tau\, e^{-j\tau^2} \quad , \qquad \tilde{a} \geq 0, \tag{16c}$$

$$L = s; \qquad \tilde{a} = \frac{\theta^2}{2} \quad . \tag{17a;17b}$$

A plot of $F[kL\tilde{a}]$ is illustrated in [Kouyoumjian and Pathak,1974]. The physical significance of the geometric quantities θ and s is shown in Figure 4. Turning next to the evaluation of I_2 in (9c) for the shadow region, it is observed that the integrals in (9c) may be simplified by employing the Debye approximation of (11) for $H^{(2)}_{\nu(\tau)}(k\rho)$ in the integrands. $\nu(\tau) = ka + m\tau \sim O(ka)$ in the transition region, and the major contribution to the integrals is for τ small; hence, one may use $\sin\gamma \approx s/\rho$ in the Debye approximation to obtain,

$$H^{(2)}_{\nu(\tau)}(k\rho) \sim \sqrt{\frac{2}{\pi ks}}\, e^{-jks + j\frac{\pi}{4}}\, e^{j(ka+m\tau)\beta_s} . \tag{18}$$

Employing (18) and (7c) in (9c) leads to

$$I_2 \sim -\frac{e^{-j\frac{\pi}{4}}}{\sqrt{2\pi k}}\, \frac{e^{-jka\theta}}{\theta}\, \frac{e^{-jks}}{\sqrt{s}} - m\sqrt{\frac{2}{k}}\, e^{-jka\theta}\, \hat{P}^{s}_{h}(\xi)\, \frac{e^{-jks}}{\sqrt{s}} , \tag{19}$$

where $\hat{P}^{s}_{h}(\xi)$ are Pekeris' caret functions [Logan,1959;Bowman et. al.,1969] defined by

$$\hat{P}^{s}_{h}(\xi) = \frac{e^{-j\frac{\pi}{4}}}{\sqrt{\pi}} \int_{-\infty}^{\infty} \frac{\partial V(\tau)}{\partial w_2(\tau)}\, e^{-j\xi\tau}\, d\tau, \tag{20}$$

and the parameter ξ in the shadow region is

$$\xi = m\theta \quad (\xi > 0 \text{ in shadow}). \tag{21}$$

The subscripts s and h in (20) correspond to the TM_z and the TE_z cases, respectively. Plots of $\hat{P}^{s}_{h}(\xi)$ are illustrated in Figures 5a and 5b in terms of related functions $p^*(\xi)$ and $q^*(\xi)$. Combining the results of (19) and (16b) according to (9a) allows one to write u at a point P_s in the shadow region as

$$u(P_s) \sim -m\sqrt{\frac{2}{k}}\, e^{-jkt}\left[\frac{e^{-j\frac{\pi}{4}}}{2\xi\sqrt{\pi}}\,(1-F[kL\tilde{a}]) + \hat{P}^{s}_{h}(\xi)\right]\frac{e^{-jks}}{\sqrt{s}} \; ; \begin{cases} t = a\theta \\ \xi = m\theta \geq 0 \end{cases} . \tag{22}$$

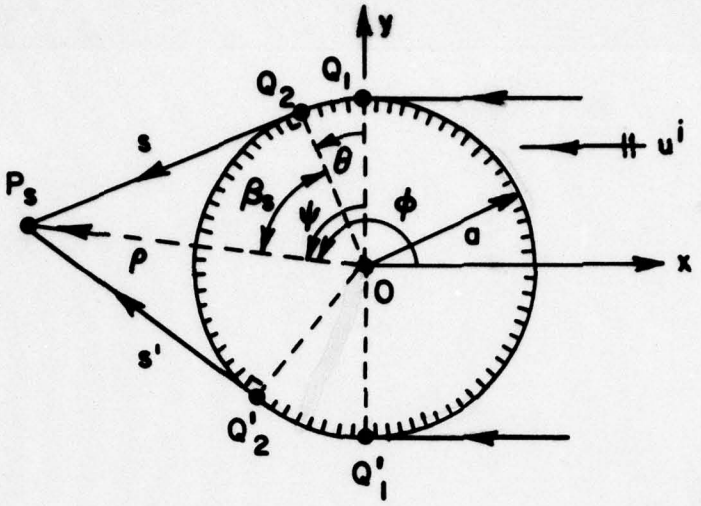

$$s^2 = \rho^2 - a^2$$

$$\beta_s = \cos^{-1}\frac{a}{\rho}$$

$$\theta = \psi - \beta_s > 0$$

Figure 4. Ray paths for the shadow region.

The above result may be interpreted geometrically as a field which propagates to P_s along the path $Q_1Q_2P_s$ after being launched by the incident wave at Q_1, as shown in Figure 4. Q_2 is the point of tangential shedding of the diffracted field from the surface. In the deep shadow region, i.e., far from SB_1, $\xi >> 0$ and $F[kL\tilde{a}] \to 1$ since $kL\tilde{a}$ becomes large; hence, for $\xi >> 0$ only the $\hat{P}_{s_h}$ term in (22) is significant. Furthermore, for $\xi >> 0$, the integral for $\hat{P}_{s_h}$ in (20) may be replaced by a rapidly convergent residue series [Logan,1959]

$$\hat{P}_{s_h}(\xi)\Big|_{\xi>>0} = \begin{cases} -\dfrac{e^{-j\frac{\pi}{4}}}{\sqrt{\pi}} \sum\limits_n \dfrac{e^{j\frac{\pi}{6}} e^{\xi q_n e^{-j\frac{5\pi}{6}}}}{2[Ai'(-q_n)]^2}, & \text{for } TM_z \text{ case} \\ -\dfrac{e^{-j\frac{\pi}{4}}}{\sqrt{\pi}} \sum\limits_n \dfrac{e^{j\frac{\pi}{6}} e^{\xi \bar{q}_n e^{-j\frac{5\pi}{6}}}}{2\bar{q}_n[Ai(-\bar{q}_n)]^2}, & \text{for } TE_z \text{ case .} \end{cases} \tag{23}$$

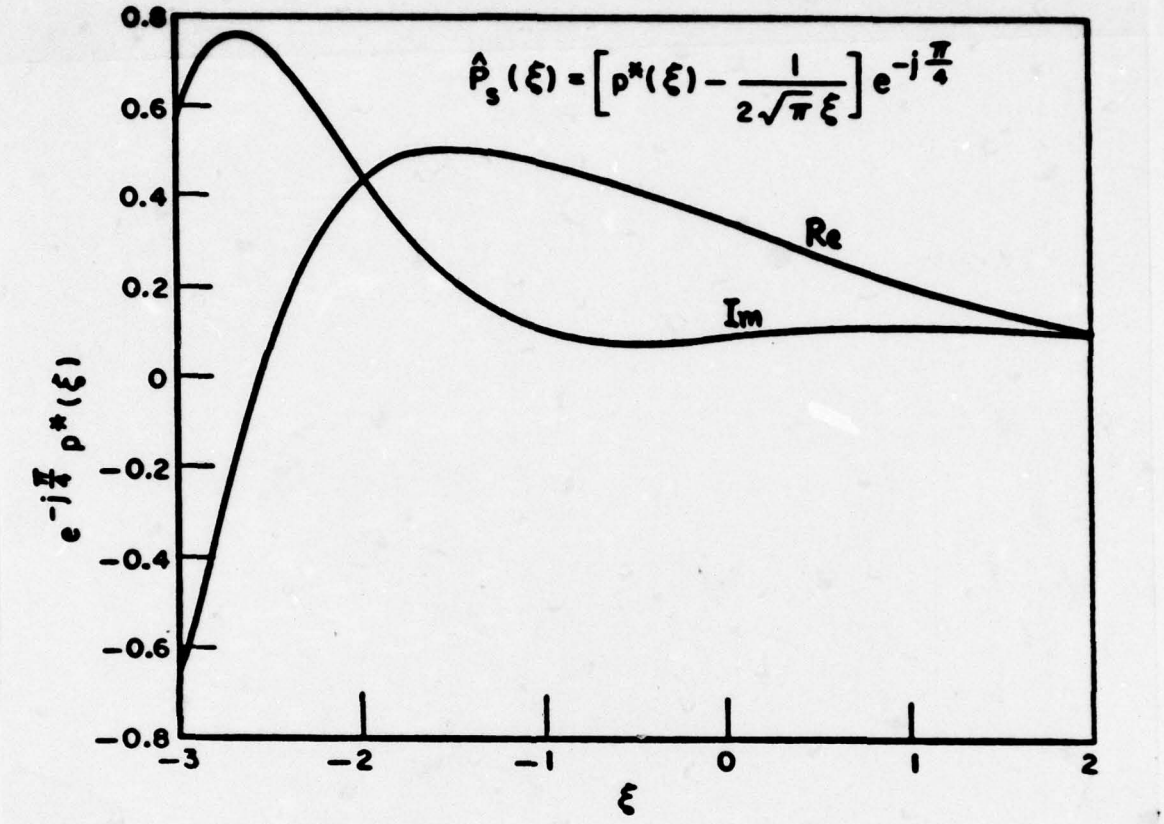

Figure 5a. Plot of $e^{-j\pi/4}p^*(\xi)$ versus ξ based on tabulated data for $p(\xi)$ by Logan (1959).

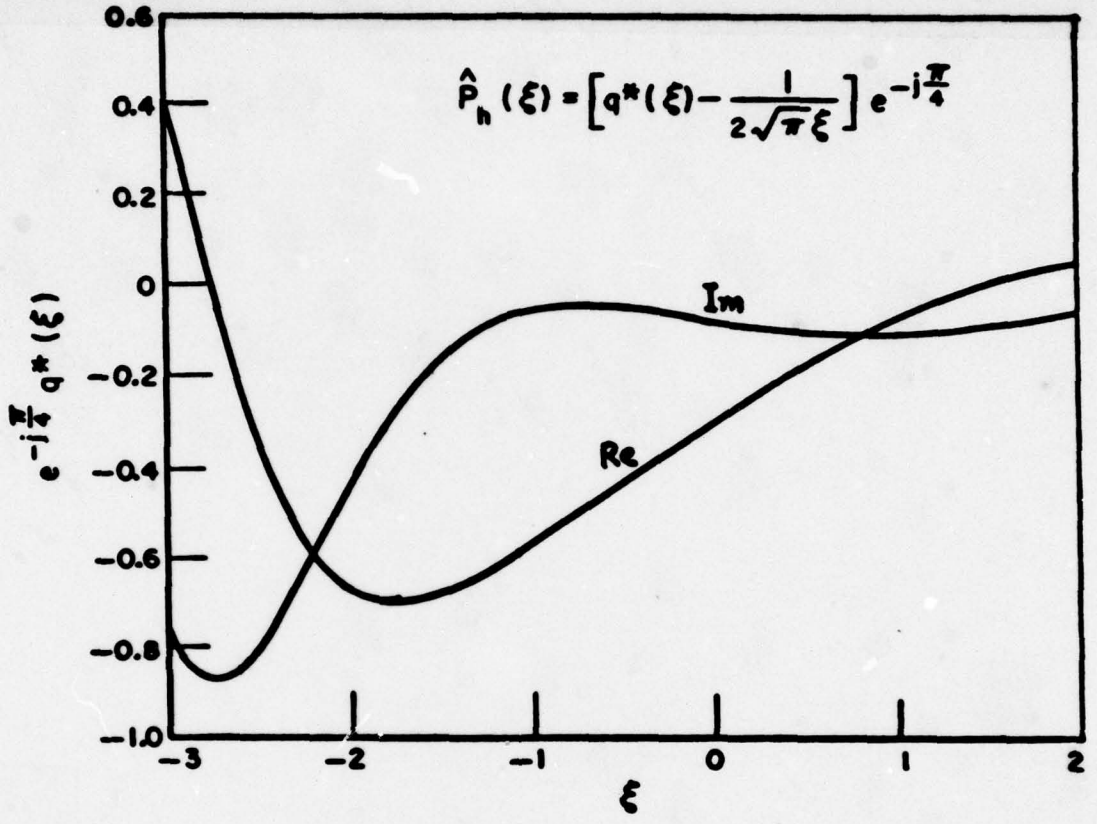

Figure 5b. Plot of $e^{-j\pi/4}q^*(\xi)$ versus ξ based on tabulated data for $q(\xi)$ by Logan (1959).

The Miller type Airy function is given by $Ai(\tau) = V(\tau)/\sqrt{\pi}$, and $Ai'(\tau) = d/d\tau\ Ai(\tau)$. The parameters q_n and $\bar{q}_n$ are defined by $Ai(-q_n) = 0$, and $Ai'(-\bar{q}_n) = 0$, respectively where $n = 1,2,3,\cdots$; their numerical values are tabulated in [Logan,1959]. Thus, far from SB_1, i.e., exterior to the shadowed transition region, (22) reduces via (23) to the Keller surface diffracted ray field given by

$$u(P_s) \sim u^i(Q_1) \left[\sum_n D_n^{s,h}(Q_1) e^{-(\alpha_n^{s,h}+jk)t} D_n^{s,h}(Q_2) \right] \frac{e^{-jks}}{\sqrt{s}} \quad . \tag{24}$$

$D_n^{s,h}$ and $\alpha_n^{s,h}$ are the Keller diffraction and attenuation coefficients for the nth surface ray mode [Keller,1956] which to first order are given by

$$[D_n^s]^2 = \sqrt{\frac{1}{2\pi k}}\ \frac{m\, e^{-j\frac{\pi}{12}}}{[Ai'(-q_n)]^2}\ ; \qquad [D_n^h]^2 = \sqrt{\frac{1}{2\pi k}}\ \frac{m\, e^{-j\frac{\pi}{12}}}{\bar{q}_n[Ai(-\bar{q}_n)]^2}\ ;$$

$$\alpha_n^s = \frac{q_n}{a}\, m\, e^{j\frac{\pi}{6}}\ ; \qquad \alpha_n^h = \frac{\bar{q}_n}{a}\ m\, e^{j\frac{\pi}{6}} \quad .$$

The superscripts s and h in (24) have the same meaning as the subscripts in (20); also $u^i(Q_1)$ is the value of the incident field at Q_1 which is unity in this case. The geometrical interpretation of (24) is the same as that in Figure 4.

Finally, the term u^{CW} corresponds to a residue series [Bowman et. al., 1969] which represents the field of multiply encircling GTD surface ray modes given by

$$u^{CW}(P_s) \sim u^i(Q_1) \left[\sum_{\ell=1}^{\infty} \sum_n D_n^{s,h}(Q_1) e^{-(\alpha_n^{s,h}+jk)(t+\ell T)} D_n^{s,h}(Q_2) \right] \frac{e^{-jks}}{\sqrt{s}} +$$

$$+ u^i(Q_1') \left[\sum_{\ell=1}^{\infty} \sum_n D_n^{s,h}(Q_1') e^{-(\alpha_n^{s,h}+jk)(t'+[\ell-1]T)} D_n^{s,h}(Q_2') \right] \frac{e^{-jks'}}{\sqrt{s'}}\ , \quad 0<\phi<\pi; \tag{25}$$

where $T = 2\pi a$; t' = arc length from Q_1' to Q_2'; and s' = distance from Q_2' to P_s. The first term in (25) is the field of surface ray modes launched at Q_1 which diffracts from the surface at Q_2 to arrive at P_s after encircling the cylinder ℓ times in the counter-clockwise sense.

The second term represents the field of surface ray modes launched at Q_1' (see Figure 4) which diffracts from Q_2 to P_S after encircling the cylinder (ℓ-1) times in the clockwise sense. For sufficiently large ka, only ℓ=1 in the second term of (25) is significant and the remaining contribution is negligible. The total field at P_S in the shadow zone is the sum of (22) and (25).

B. Field Analysis for the Illuminated Transition Region

If one directly employs the result given in the previous section for the shadow region to calculate the field u at a point P_L close to SB_1 in the lit region, then

$$u(P_L) \sim u^i(P_L) - m\sqrt{\frac{2}{k}}\, e^{-jkt}\left[\frac{e^{-j\frac{\pi}{4}}}{2\xi\sqrt{\pi}}\,(1-F[kL\tilde{a}]) + \hat{P}_{\hat{s}\hat{n}}(\xi)\right]\frac{e^{-jks}}{\sqrt{s}}\quad,$$

$$t = a\theta < 0. \tag{26}$$

Since $\phi<\phi_S$ and $\beta_D<\beta_S$ in the lit region $H(\phi-\phi_S) = 0$ in (14). Also, (19) is unchanged except that ξ,t and θ now become negative in the lit region. The second term in (26) may be interpreted as a scattered field which after being launched at Q_1 propagates backwards from Q_1 to Q_3 before being shed tangentially from Q_3 to P_L as illustrated in Figure 6.

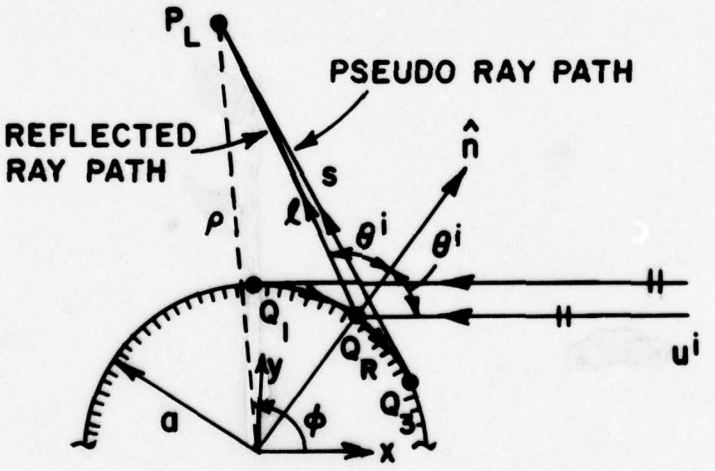

Figure 6. Reflected and pseudo ray paths for the lit region.

It is noted from Figure 6 that this "pseudo ray" propagation path is different from the geometric optical reflected ray path which satisfies the generalized Fermat's principle. The result in (26) is quite accurate very close to SB_1; however, just as the result in [Fock,1951] and [Wait and Conda,1959], this result also does not reduce to the geometric optical ray field far from SB_1. An approximation for $H_\nu^{(2)}(k\rho)$ which is different from that in (18) appears to be necessary to adequately approximate the field behavior in the deep lit region. The following approximate procedure is adopted to achieve this goal. First, $H_{\nu(\tau)}^{(2)}(k\rho)$ in I_2 of (9c) is replaced by its large argument approximation ($\nu(\tau)<<k\rho$) such that

$$I_2 \approx \sqrt{\frac{2}{\pi k\rho}}\, e^{-j\left(k\rho - \frac{\pi}{4}\right)} \left[jm \int_{c_2} d\tau \frac{\partial V(\tau)}{\partial w_2(\tau)} e^{j\nu(\tau)\left(\frac{\pi}{2} - \psi\right)} \right.$$

$$\left. + \frac{m}{2} \int_{c_1} d\tau \frac{\partial w_1(\tau)}{\partial w_2(\tau)} e^{j\nu(\tau)\left(\frac{\pi}{2} - \psi\right)} \right]. \qquad (27)$$

One next defines the following

$$\frac{\pi}{2} - \psi = 2\tilde{\gamma} \; ; \qquad \xi' = -2m \sin\tilde{\gamma} \; , \qquad (28a;28b)$$

where

$$-\tilde{\gamma} = \sin^{-1}\frac{\xi'}{2m} = \left(\frac{1}{2m}\right)(\xi') + \frac{1}{6}\left(\frac{1}{2m}\right)^3(\xi')^3 + \frac{3}{40}\left(\frac{1}{2m}\right)^5(\xi')^5 + \cdots \; ; \qquad (29)$$

with

$$\left(\frac{\xi'}{2m}\right)^2 < 1.$$

In the transition region, ξ' may be assumed to be small in comparison to m which is taken to be large. One may approximate $\nu(\tau)(\pi/2 - \psi)$ in the exponent of (27) via (29) as

$$\nu(\tau)\left(\frac{\pi}{2} - \psi\right) = (ka + m\tau)2\tilde{\gamma} \approx -ka\left[\frac{\xi'}{m} + \frac{1}{24}\frac{(\xi')^3}{m^3}\right] - \tau\xi' \; . \qquad (30)$$

Incorporating this result into (27) yields

$$I_2 \sim -\sqrt{\frac{2}{k\rho}}\, e^{-jk\rho}\left[me^{j2ka\,\sin\tilde{\gamma}-j\frac{(\xi')^3}{12}} \left(\frac{e^{-j\frac{\pi}{4}}}{2\xi'\sqrt{\pi}} + \frac{e^{-j\frac{\pi}{4}}}{\sqrt{\pi}} \int_{-\infty}^{\infty} d\tau \right.\right.$$

$$\left.\left. \cdot \frac{\partial V(\tau)}{\partial w_2(\tau)}\, e^{-j\xi'\tau} \right)\right] . \qquad (31)$$

Referring to Figure 6, it is seen that in the far zone ($k\rho >> ka$)

$$\phi \approx 2\theta^i;\ \rho \approx \begin{cases} \ell, \text{ in amplitude} \\ \ell + a\cos\theta^i, \text{ in phase} \end{cases} \qquad (32a;32b)$$

$$2\tilde{\gamma} = \pi - |\phi| \approx \pi - 2\theta^i \qquad (32c)$$

respectively. Thus, I_2 may be expressed in terms of the reflected ray coordinates as

$$I_2 \sim -\sqrt{\frac{2}{k\ell}}\, e^{-jk(\ell + a\cos\theta^i)}\, me^{j2ka\,\cos\theta^i - j\frac{(\xi')^3}{12}} \left[\frac{e^{-j\frac{\pi}{4}}}{2\sqrt{\pi}\,\xi'} + \hat{P}_{s_h}(\xi') \right]; \qquad (33)$$

$$\xi' = -2\,m\cos\theta^i \text{ (via (28b) and (32c))}. \qquad (34)$$

Turning next to the evaluation of I_1 of (9b), one begins with its integral representation in (12). The contour c_B is deformed into the SDP through the saddle point β_s as in Figure 3; the pole at β_p is not crossed in this contour deformation since $\beta_p < \beta_s$ is in the lit region. To be consistent with (27), I_1 will also be evaluated in the far zone; thus, $\beta_s = \cos^{-1} a/\rho \approx \pi/2$ for $k\rho >> ka$ so that a three term Taylor expansion about β_s for the exponent in (12) yields

$$I_1 \approx u^i(P_L) - \frac{e^{jka(\frac{\pi}{2} - \psi)}}{2\pi j} e^{-jk\rho} \int_{SDP} d\beta \frac{e^{k\rho[\frac{j}{2}(\beta - \frac{\pi}{2})^2]}}{\beta - \beta_p} \quad . \qquad (35)$$

The integral in (34) may also be directly expressed in terms of the F function of (16d) which contains the Fresnel integral as done previously for the SDP integral of (14) for the shadow zone.

$$I_1 \sim u^i(P_L) - \frac{e^{-j(k\rho + \frac{\pi}{4})}}{\sqrt{2\pi k\rho}} \frac{e^{jka\, 2\tilde{\gamma}}}{2\tilde{\gamma}} F[k\rho \cdot 2\tilde{\gamma}^2] \qquad (36)$$

Incorporating (29), and the far zone approximations for ρ and ϕ of (32) into (35) yields the following result.

$$I_1 \sim u^i(P_L) + m \frac{e^{-j\frac{\pi}{4}}}{\sqrt{2\pi k}\xi'} e^{j2ka\cos\theta^i - j\frac{(\xi')^3}{12}} F[kL'\tilde{a}'] \frac{e^{-jk(\ell + a\cos\theta^i)}}{\sqrt{\ell}} ;$$

$$k\rho >> ka, \qquad (37)$$

$$L' = \ell \; ; \; \tilde{a}' = \frac{(\xi')^2}{2m^2} = 2\cos^2\theta^i \text{ (with } \xi' \text{ as in (34))}. \qquad (38a;38b)$$

Combining (33) and (37) according to (9a) gives $u(P_L)$ in the far zone as

$$u(P_L) \sim u^i(P_L) + u^i(Q_R) \left[-m\sqrt{\frac{2}{k}} e^{-j\frac{(\xi')^3}{12}} \left\{ \frac{e^{-j\frac{\pi}{4}}}{2\xi'\sqrt{\pi}} (1 - F[kL'\tilde{a}']) + \hat{P}_{s_h}(\xi') \right\} \right] \frac{e^{-jk\ell}}{\sqrt{\ell}} , \qquad (39a)$$

which for later convenience is re-expressed as

$$u(P_L) \sim u^i(P_L) + u^i(Q_R)\left[-\sqrt{-\frac{4}{\xi'}}\, e^{-j\frac{(\xi')^3}{12}} \left\{\frac{e^{-j\frac{\pi}{4}}}{2\xi'\sqrt{\pi}}\,(1-F[kL'\tilde{a}'])\right.\right.$$

$$\left.\left. + \hat{P}_{\substack{s\\h}}(\xi')\right\}\right]\sqrt{\frac{\tilde{\rho}^{\gamma}}{\ell}}\, e^{-jk\ell}\,, \qquad (39b)$$

where

$$u^i(Q_R) = \text{incident field at } Q_R \text{ (see Figure 6)} = e^{jka\cos\theta^i}\,;$$

$$\tilde{\rho}^{\gamma} = \frac{a\cos\theta^i}{2} = \text{reflected ray caustic distance.} \qquad (39c)$$

Far from SB_1 in the lit region, $\xi'<<0$, and hence $F[kL'\tilde{a}'] \to 1$; furthermore, $\hat{P}_{\substack{s\\h}}(\xi')$ may be asymptotically approximated as [Logan,1959; Logan and Yee,1962]

$$\hat{P}_{\substack{s\\h}}(\xi') \sim \pm\sqrt{\frac{-\xi'}{4}}\; e^{j\frac{(\xi')^3}{12}}\; [1 + O(\xi'^{-3})]; \qquad \xi'<<0. \qquad (40)$$

Thus, incorporating (40) into (39b) for the deep lit region ($\xi'<<0$) yields

$$u(P_L) \sim u^i(P_L) \mp u^i(Q_R)\sqrt{\frac{\tilde{\rho}^{\gamma}}{\ell}}\, e^{-jk\ell}\,, \quad \text{for the} \left\{\begin{matrix} TM_z \\ TE_z \end{matrix}\right\} \text{case.} \qquad (41)$$

The field u^{GO} of the geometric optical incident and reflected rays represents an accurate, first order asymptotic field approximation within the deep lit region, and it is well known to be

$$u^{GO}(P_L) \sim u^i(P_L) + u^i(Q_R)\; R_{\substack{s\\h}}\sqrt{\frac{\tilde{\rho}^{\gamma}}{\tilde{\rho}^{\gamma}+\ell}}\; e^{-jk\ell} \qquad (42)$$

in which $R_{\substack{s\\h}}$ is the surface reflection coefficient given by $\begin{cases} R_s=-1 \text{ for } TM_z \text{ case} \\ R_h=+1 \text{ for } TE_z \text{ case.} \end{cases}$ It is apparent from (42) that the result in (41) is the far zone geometric optics field, since the reflected ray divergence factor $\sqrt{\hat{\rho}^\gamma/(\hat{\rho}^\gamma+\ell)}$ of (42) reduces to $\sqrt{\hat{\rho}^\gamma/\ell}$ in the far zone ($\ell>>\hat{\rho}^\gamma$). The result in (39) for the lit region has essentially the same form as (22) for the shadow; this is a desirable feature since the results in (22) and (39) are in terms of tabulated functions, and they admit a simple interpretation which will be discussed in Section V. The far zone result of (41), and hence (39) may therefore be heuristically generalized to the near zone (which is exterior to the close vicinity of the surface) according to ray-optics, by replacing the far zone ray divergence factor $\sqrt{\hat{\rho}^\gamma/\ell}$ with it's near zone value $\sqrt{\hat{\rho}^\gamma/(\hat{\rho}^\gamma+\ell)}$, where ℓ must now represent the near zone reflected ray distance from Q_R to P_L. Thus, the near zone result for the lit region is

$$u(P_L) \sim u^i(P_L) + u^i(Q_R)\left[-\sqrt{\frac{-4}{\xi'}}\, e^{-j\frac{(\xi')^3}{12}}\left\{\frac{e^{-j\frac{\pi}{4}}}{2\xi'\sqrt{\pi}}\,(1-F[kL'\hat{a}'])+\hat{P}_{\substack{s\\h}}(\xi')\right\}\right] \cdot \sqrt{\frac{\hat{\rho}^\gamma}{\hat{\rho}^\gamma+\ell}}\; e^{-jk\ell};\quad \xi' = -2m\cos\theta^i \leq 0;\quad L'=\ell+\hat{\rho}^\gamma. \tag{43}$$

It is observed via (22) that the distance parameter L for the shadow zone is the distance s from the caustic point Q_2 to the field point P_s. The caustic at Q_2 is the effective origin of the diffracted ray path to P_s. Thus, keeping this interpretation in mind, one modifies $L'=\ell$ in (38a) for the far zone to $L'=\ell+\hat{\rho}^\gamma$ in (43) for the near zone, since $\ell+\hat{\rho}^\gamma$ is now the distance to P_L from the virtual caustic of the reflected ray path along which the field $u(P_L)$ is assumed to propagate. One notes that L' of (43) reduces to that of (38a) at the shadow boundary, and also in the far zone (where $\ell>>\hat{\rho}^\gamma$). The value of L' is significant only near the shadow boundary where L' of (43) and (38a) are approximately the same; hence one could use L' of either (43) or (38a) without noticeably affecting the numerical calculations. The expression in (43) now properly reduces to (42) in the deep lit region. The total field at P_L is the sum of (43) and u^{cw} of (25) with P_s replaced by P_L; however, u^{cw} is negligible in the lit region for large ka.

It will be shown in Section V that (43) for the lit region and (22) for the shadow region are equal at the shadow boundary, thereby making the asymptotic solution presented in this paper continuous from the deep lit region to the deep shadow.

III. GENERALIZATION TO THE SMOOTH CONVEX CYLINDER CASE

The uniform results for the circular cylinder in (22) and (43) may be readily generalized to treat the scattering by a convex cylinder of slowly varying curvature in the usual manner, by utilizing the local properties of propagation, scattering and diffraction of waves at high frequencies. Thus, one treats each point on the convex cylinder as if it were locally on a circular cylinder of the same radius of curvature, i.e., the radius (a) in the solution of the previous section is replaced by ρ_g where ρ_g is now the local radius of curvature of the convex cylinder. Specifically, the generalization of (22) and (43) to the case of plane wave scattering by a smooth, perfectly-conducting convex cylinder of variable curvature is indicated below for the shadow region in part A, and for the lit region in Part B.

A. Shadow Region

The field u at P_s in the shadow zone of the convex cylinder becomes

$$u(P_s \sim u^i(Q_1)\left[-\sqrt{m(Q_1)}\sqrt{m(Q_2)}\; e^{-jkt}\sqrt{\frac{2}{k}}\left\{\frac{e^{-j\frac{\pi}{4}}}{2\xi\sqrt{\pi}}\,(1-F[kL\tilde{a}])+\hat{P}_{s_h}(\xi)\right\}\right]\frac{e^{-jks}}{\sqrt{s}}\;;\;\xi\geq 0 \tag{44a}$$

with

$$\xi=\int_{Q_1}^{Q_2}\frac{m(t')}{\rho_g(t')}\,dt'\;;\qquad t=\int_{Q_1}^{Q_2}dt'\;;\qquad m(t')=\left[\frac{k\rho_g(t')}{2}\right]^{1/3} \tag{44b,44c,44d}$$

and

$$L=s\;;\qquad \tilde{a}=\xi^2/[2\,m(Q_1)m(Q_2)]\quad. \tag{44e;44f}$$

The points Q_1 and Q_2 are indicated in Figure 1; t' denotes any point between Q_1 and Q_2 on the cylinder and s is the distance from Q_2 to P_s. It is noted that m in (22) is replaced by $\sqrt{m(Q_1)}\sqrt{m(Q_2)}$ in (44a) to be consistent with reciprocity, since the point of grazing incidence Q_1 and the point of diffraction Q_2 on the convex surface in general possess different radii of curvatures $\rho_g(Q_1)$ and $\rho_g(Q_2)$, respectively. This symmetrical splitting of m is also essential for preserving the uniform property of the result so that deep in the shadow region where $\xi\gg 0$, (44a) reduces to the GTD result of (24) (except that $(\alpha_n^{s_h}\, t)$ therein is replaced by $\int_{Q_1}^{Q_2}\alpha_n^{s_h}(t')dt'$ for the convex cylinder).

B. Lit Region

The field u at P_L in the lit zone of the convex cylinder becomes

$$u(P_L) \sim u^i(P_L) + u^i(Q_R)\left[-\sqrt{\frac{-4}{\xi'}}\, e^{-j\frac{(\xi')^3}{12}} \left\{\frac{e^{-j\frac{\pi}{4}}}{2\xi'\sqrt{\pi}}\,(1-F[kL'\tilde{a}'])+\hat{P}_{s_h}(\xi')\right\}\right] \cdot \sqrt{\frac{\tilde{\rho}^{\gamma}}{\tilde{\rho}^{\gamma}+\ell}}\, e^{-jk\ell}; \quad \xi' \leq 0, \tag{45a}$$

with

$$\xi' = -2\, m(Q_R)\cos\theta^i\ ; \qquad m(Q_R) = \left[\frac{k\rho_g(Q_R)}{2}\right]^{1/3}\ ; \quad \tilde{\rho}^{\gamma} = \frac{\rho_g(Q_R)\cos\theta^i}{2}\ ; \tag{45b;45c;45d}$$

and

$$L' = \ell + \tilde{\rho}^{\gamma}; \quad \tilde{a}' = 2\cos^2\theta^i. \tag{45e;45f}$$

The point of reflection Q_R is shown in Figure 1; also ℓ is the distance from Q_R to P_L as before. Deep in the lit zone where $\xi' << 0$, (45a) reduces to the geometrical optics result of (42) except that $\tilde{\rho}^{\gamma}$ is now given more generally by (45d) for the convex cylinder.

IV. FIELD IN THE CLOSE NEIGHBORHOOD OF A SMOOTH CONVEX CYLINDER

While the uniform result in (44) and (45) for the scattering of a plane wave by a smooth, perfectly conducting convex cylinder is valid in the far and near zone of the surface, it is not valid in the close neighborhood of the surface. The region of validity of (44) and (45) excludes the boundary layer and it's vicinity in the shadow region, and it excludes approximately the same distance from the surface in the lit region. The field in the close neighborhood of the surface is available elsewhere in terms of the canonical Fock integral [Logan and Yee,1962;Ivanov,1971] which is very complicated for numerical calculations. In this section a Taylor series approximation for the canonical Fock integral is obtained to describe the field in the close neighborhood of the surface. This approximation is very convenient for numerical calculations.

When the field point is extremely close to the surface of a circular cylinder such that $k(\rho-a)<<ka$, one may then approximate $J_{\nu(\tau)}(k\rho)$ and $H^{(2)}_{\nu(\tau)}(k\rho)$ in (8a) and (8b) by

$$J_\nu(k\rho) \approx (m\sqrt{\pi})^{-1} V(\tau-h); \quad H^{(1)}_\nu(k\rho) \approx \mp j(m\sqrt{\pi})^{-1} w_{1_2}(\tau-h) \qquad (46a);(46b)$$

where

$$h = m^{-1}kd; \qquad d = \rho - a. \qquad (46c);(46d)$$

Incorporating the above results into (8a) and (8b) essentially yields an expression for the field u in terms of Fock's canonical integral as:

$$u \approx \frac{e^{-jka\psi}}{\sqrt{\pi}} \int_{-\infty-j\varepsilon}^{\infty-j\varepsilon} d\tau \left[V(\tau-h) - \frac{\partial V(\tau)}{\partial W_2(\tau)} w_2(\tau-h)\right] e^{-jZ\tau}; \quad Z = m\psi \qquad (47a)$$

or

$$u \approx \frac{-j}{2\sqrt{\pi}} e^{-jka\psi} \int_{-\infty-j\varepsilon}^{\infty-j\varepsilon} d\tau \left[w_1(\tau-h) - \frac{\partial W_1(\tau)}{\partial W_2(\tau)} w_2(\tau-h)\right] e^{-jZ\tau}; \quad Z=m\psi, \qquad (47b)$$

with $\psi = |\phi| - \pi/2$ as before.

The above integrals for the circular cylinder case will be approximated in the close vicinity of the surface by a Taylor series in direct powers of the normalized distance h; these results will then be generalized to the convex cylinder case as in section III.

The $\psi>0$ case will be considered first, to be followed by a similar treatment for the $\psi<0$ case. Let $0<\phi<\pi$ as in section II; the results for $\pi<\phi<2\pi$ may be directly obtained via symmetry. For $\psi>0$, it is convenient to employ the representation in (47b). Thus, for h small, one may represent $w_{1/2}(\tau-h)$ in (47b) by a Taylor series,

$$w_{1/2}(\tau-h) = w_{1/2}(\tau) - w'_{1/2}(\tau)h + \tau w_{1/2}(\tau)\frac{h^2}{2} - [w_{1/2}(\tau) + \tau w'_{1/2}(\tau)]\frac{h^3}{6}$$
$$+ [2w'_{1/2}(\tau) + \tau^2 w_{1/2}(\tau)]\frac{h^4}{24} - [4\tau w_{1/2}(\tau) + \tau^2 w'_{1/2}(\tau)]\frac{h^5}{120} + O(h^6) \quad (48)$$

where the primes on $w_{1/2}(\tau)$ denote differentiation with respect to τ. Incorporating (48) into (47b) allows one to express u in terms of Fock current functions and it's derivatives.

$$u(P)\Big|_{\psi>0} \approx e^{-jka\psi}\left[h\tilde{g}(Z) + \frac{jh^3}{3!}\tilde{g}'(Z) - \frac{2h^4}{4!}\tilde{g}(Z) - \frac{h^5}{5!}\tilde{g}''(Z)\right] + O(h^6);$$

for the soft or TM_z case ($\hat{Q}=1$ case) (49a)

$$u(P)\Big|_{\psi>0} \approx e^{-jka\psi}\left[g(Z) + \frac{jh^2}{2!}g'(Z) - \frac{h^3}{3!}g(Z) - \frac{h^4}{4!}g''(Z) - \frac{j4h^5}{5!}g'(Z)\right]$$
$$+ O(h^6); \text{ for the hard or } TE_z \text{ case } (\hat{Q} = \partial/\partial\tau \text{ case}). \quad (49b)$$

$\tilde{g}(D)$ and $g(D)$ are the Fock functions [Fock,1946;Logan,1959] defined by

$$\tilde{g}(D) = \frac{1}{\sqrt{\pi}}\int_{-\infty-j\varepsilon}^{\infty-j\varepsilon} d\tau \frac{e^{-jD\tau}}{w_2(\tau)} \; ; \quad g(D) = \frac{1}{\sqrt{\pi}}\int_{-\infty-j\varepsilon}^{\infty-j\varepsilon} d\tau \frac{e^{-jD\tau}}{w'_2(\tau)} \; . \quad (50a;50b)$$

The values of $\tilde{g}(D)$ and $g(D)$ are extensively tabulated [Logan,1959]. The primes on $\tilde{g}(D)$ and $g(D)$ in (49a;b) denote differentiation with respect to the argument (D). The derivatives of $\tilde{g}$ and g may be evaluated numerically from the interpolated values of g and g, respectively. In obtaining (49a;b), use has been made of the well-known relationships $w''_{1/2}(\tau) = \tau w_{1/2}(\tau)$;

$w_1'(\tau)w_2(\tau)-w_1(\tau)w_2'(\tau)=-2j$; and $\int_{-\infty-j\varepsilon}^{\infty-j\varepsilon} d\tau\, e^{-jD\tau}\, \tau^n f(\tau) = j^n \frac{\partial^n}{\partial D^n} \int_{-\infty-j\varepsilon}^{\infty-j\varepsilon} d\tau\, e^{-jD\tau}\, f(\tau)$,

where $f(\tau)$ represents some combination of the Airy functions. It is noted that $\tilde{g}(Z)e^{-jka\psi}$ and $g(Z)e^{-jka\psi}$ are directly proportional to the electric current density induced on the cylinder surface by the incident plane wave [Fock,1946]. In the present case, these currents exist at P_N which is the normal projection on the surface of the field point P exterior to the surface. For $\psi>0$, the point P_N lies in the shadow zone. The distance from P_N to P is $d(=\rho-a)$; furthermore, the unit outward surface normal at P_N is $\hat{\rho} = \hat{n} = \overrightarrow{P_NP}/\overline{P_NP}$. When the point P_N on the surface lies in the deep shadow ($\psi>>0$ and hence $Z>>0$), the Fock currents $\tilde{g}\, e^{-jka\psi}$ and $g\, e^{-jka\psi}$ reduce uniformly to the GTD current representation [Pathak and Kouyoumjian,1974].

For $\psi<0$, it is convenient to begin by re-writing (47a) in terms of a new parameter Z' as employed for the Fock currents by Logan (1959).

$$Z' = m\sin\psi = -m\cos\phi;\quad \psi = \sin^{-1}\frac{Z'}{m} = \frac{Z'}{m} + \frac{1}{6}\frac{(Z')^3}{m^3} + \cdots,\quad \text{if } \left(\frac{Z'}{m}\right)^2<1. \tag{51a,51b}$$

The approximation in (51b) is valid within the shadow boundary transition region for large m. Thus, (47a) becomes

$$u(P)\big|_{\psi<0} \approx e^{jka\cos\phi}\frac{e^{-j(Z')^3/3}}{\sqrt{\pi}} \int_{-\infty-j\varepsilon}^{\infty-j\varepsilon} d\tau \left[V(\tau-h) - \frac{\partial V(\tau)}{\partial w_2(\tau)} w_2(\tau-h)\right] e^{-jZ'\tau}; \tag{52a}$$

or

$$u(P)_{\psi<0} \approx e^{jka\cos\phi}\left[e^{-jhZ'} - \frac{e^{-j(Z')^3/3}}{\sqrt{\pi}} \int_{-\infty-j\varepsilon}^{\infty-j\varepsilon} d\tau\, \frac{\partial V(\tau)}{\partial w_2(\tau)}\, w_2(\tau-h)e^{-jZ'\tau}\right]. \tag{52b}$$

In obtaining (52a), one employs $e^{-jZ\tau} \approx e^{-jZ'\tau}$ and $e^{-jka\psi} \approx e^{jka\cos\phi - j(Z')^3/3}$. Furthermore employing

$$\frac{1}{\sqrt{\pi}} \int_{-\infty-j\varepsilon}^{\infty-j\varepsilon} d\tau\, V(\tau-h) e^{-jZ'\tau} = e^{-jhZ'}\, e^{j(Z')^3/3}$$

for $\psi<0$ in (52a) leads to (52b). Next, the $w_2(\tau-h)$ in (52b) may be expanded for small h as in (48) to arrive at an expression similar to that in (49a;b) for u in terms of the Fock currents and it's derivatives,

$$u(P)\big|_{\psi<0} \approx e^{jka\cos\phi}\left[e^{-jhZ'} - \left(\sum_{n=0}^{5} (-1)^n \frac{(jhZ')^n}{n!}\right)\right.$$

$$\left. + e^{-j(Z')^3/3}\left\{h\tilde{g}(Z') + \frac{jh^3}{3!}\tilde{g}'(Z') - \frac{2h^4}{4!}\tilde{g}(Z') - \frac{h^5}{5!}\tilde{g}''(Z')\right\}\right],$$

$$+ O(h^6), \text{ for the soft or } TM_z \text{ case } (\tilde{Q}=1 \text{ case}), \qquad (53a)$$

$$u(P)\big|_{\psi<0} \approx e^{jka\cos\phi}\left[e^{-jhZ'} - \left(\sum_{n=0}^{5} \frac{(-1)^n}{n!}(jhZ')^n\right)\right.$$

$$\left. + e^{-j(Z')^3/3}\left\{g(Z') + \frac{jh^2}{2!}g'(z') - \frac{h^3}{3!}g(Z') - \frac{h^4}{4!}g''(Z') - \right.\right.$$

$$\left.\left. - j\frac{4h^5}{5!}g'(Z')\right\}\right] + O(h^6), \text{ for the hard or } TE_z \text{ case } \left(\tilde{Q} = \frac{\partial}{\partial\tau} \text{ case}\right)$$

(53b)

For $\psi<0$, the point P_N on the surface is in the lit zone, where P_N is the normal projection on the surface of the field point P, as indicated previously. The Fock currents $e^{jka\cos\phi - j(Z')^3/3}\, g(Z')$ and $e^{jka\cos\phi - j(Z')^3/3}\, \tilde{g}(Z')(-j/m(P_N))$ at P_N which are induced by the incident plane wave reduce uniformly to the geometrical optics currents when P_N moves into the deep illuminated region $(Z'<<0)$.

The results in (49a;b) and (53a;b) may now be generalized as in section III to obtain the field u in the close neighbourhood of a smooth, perfectly conducting convex cylinder illuminated by a plane wave. Thus,

$$u(P) \approx U_o e^{-j\Omega}\left[T_1+T_2\left\{h\tilde{g}(D)+\frac{jh^3}{3!}\tilde{g}'(D)-\frac{2h^4}{4!}\tilde{g}(D)-\frac{h^5}{5!}\tilde{g}''(D)\right\}\right]+O(h^6),$$

for the soft or TM_z case, (54a)

$$u(P) \approx U_o e^{-j\Omega}\left[T_1+T_2\left\{g(D)+\frac{jh^2}{2!}g'(D)-\frac{h^3}{3!}g(D)-\frac{h^4}{4!}g''(D)-\frac{j4h^5}{5!}g'(D)\right\}\right]+O(h^6)$$

for the hard or TE_z case, (54b)

where

$$U_o=\begin{Bmatrix} u^i(Q_1) \\ u^i(P_N)\end{Bmatrix};\quad \Omega=\begin{Bmatrix} k\int_{Q_1}^{P_N} dt' \\ 1\end{Bmatrix};\quad D=\begin{Bmatrix} \int_{Q_1}^{P_N}\rho\frac{m(t')}{g(t')}dt' \\ -m(P_N)\cos\theta^i\end{Bmatrix};\quad \text{for}\begin{Bmatrix} P_N \text{ in shadow zone} \\ P_N \text{ in lit zone}\end{Bmatrix}$$

(55a;55b;55c)

and

$$T_1=\begin{Bmatrix} 0 \\ e^{-jhD}-\sum_{n=0}^{5}\frac{(-1)^n}{n!}(jhD)^n\end{Bmatrix};\quad T_2=\begin{Bmatrix}\left[\frac{\rho_g(P_N)}{\rho_g(Q_1)}\right]^{1/6} \\ e^{-j\frac{D^3}{3}}\end{Bmatrix};\quad \text{for}\begin{Bmatrix} P_N \text{ in shadow zone} \\ P_N \text{ in lit zone}\end{Bmatrix}$$

(55d;55e)

The arc length integrals in (55b) and (55c) are evaluated along the surface geodesic from Q_1 to P_N in the shadow region; whereas, θ^i is the acute angle between the incident ray and the surface normal to P_N in the lit region. While the definitions for u_o, Ω and D for the convex cylinder follow fairly directly from the generalizations of the quantities in (49a,b) and (53a;b) for the circular case, the introduction of $[\rho_g(P_N)/\rho_g(Q_1)]^{1/6}$ in T_2 for P_N in the shadow is required to preserve the uniform nature of the Fock currents in the shadow zone of the convex cylinder [Pathak and Kouyoumjian,1974].

V. NUMERICAL RESULTS AND DISCUSSION

A uniform asymptotic result for the near zone field exterior to a perfectly conducting convex cylinder which is illuminated by a plane wave as shown in Figure 1, is given in (44a) and (45a) for the shadow and lit zones, respectively. These results may be employed via reciprocity to directly obtain the radiation patterns of electric or magnetic line sources in the near zone of the cylinder. A few numerical results for the radiation patterns of line sources near circular and elliptic cylinders which are based on (44a) and (45a) are presented in Figures 7b, 7c and 7d. The accuracy of this uniform result is confirmed by the excellent agreement obtained between the present solution and the eigenfunction solution for the circular cylinder case. Similar agreement is observed for the elliptic cylinder examples in which case the present result is compared with a moment method solution. The results in (44a) and (45a) are not valid in the close vicinity of the surface; hence, the results in (53a) and (53b) may be used to calculate the field in the close neighborhood of the surface. In particular, the latter results are used to calculate the far zone fields of line sources in the close vicinity of a circular cylinder via reciprocity as shown in Figures 8a and 8b. It is seen that these results tend to blend with those obtained via (44a) and (45a) thereby providing an overlap region for these two representations. It is noted from the above pattern calculations that the uniform result of (44a) and (45a) makes the leading term of the total high frequency field continuous at the shadow boundaries. On the other hand, the use of the usual ray optical or GTD solution would have produced a discontinuity in the field pattern at the shadow boundaries. One may verify the continuity property of the uniform result as follows. Near a shadow boundary, ξ and ξ' must both approach zero since the arc length $t \to 0$, and $\theta^i \to \pi/2$. Furthermore,

$$F(\sigma) \to \left[\sqrt{\pi\sigma} - 2\sigma e^{j\frac{\pi}{4}}\right] e^{j(\frac{\pi}{4} + \sigma)} \quad \text{as } \sigma \to 0, \tag{56a}$$

and one may re-express $\hat{P}_{\substack{s \\ h}}$ as

$$\hat{P}_{\substack{s \\ h}}(\sigma) = \left[\begin{Bmatrix} p^*(\sigma) \\ q^*(\sigma) \end{Bmatrix} - \frac{1}{2\sqrt{\pi\sigma}}\right] e^{-j\frac{\pi}{4}} \quad . \tag{56b}$$

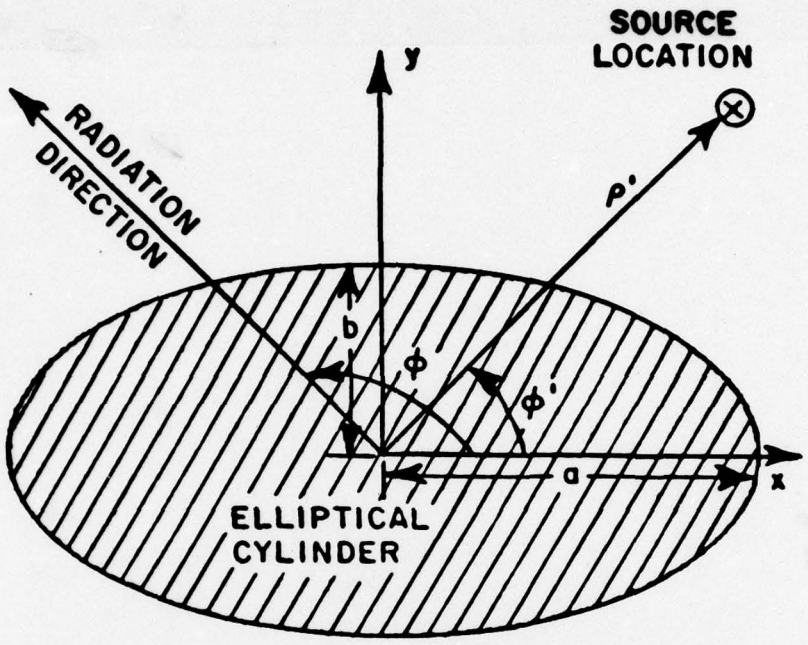

Figure 7a. Elliptic cylinder configuration excited by a 2-D line source.

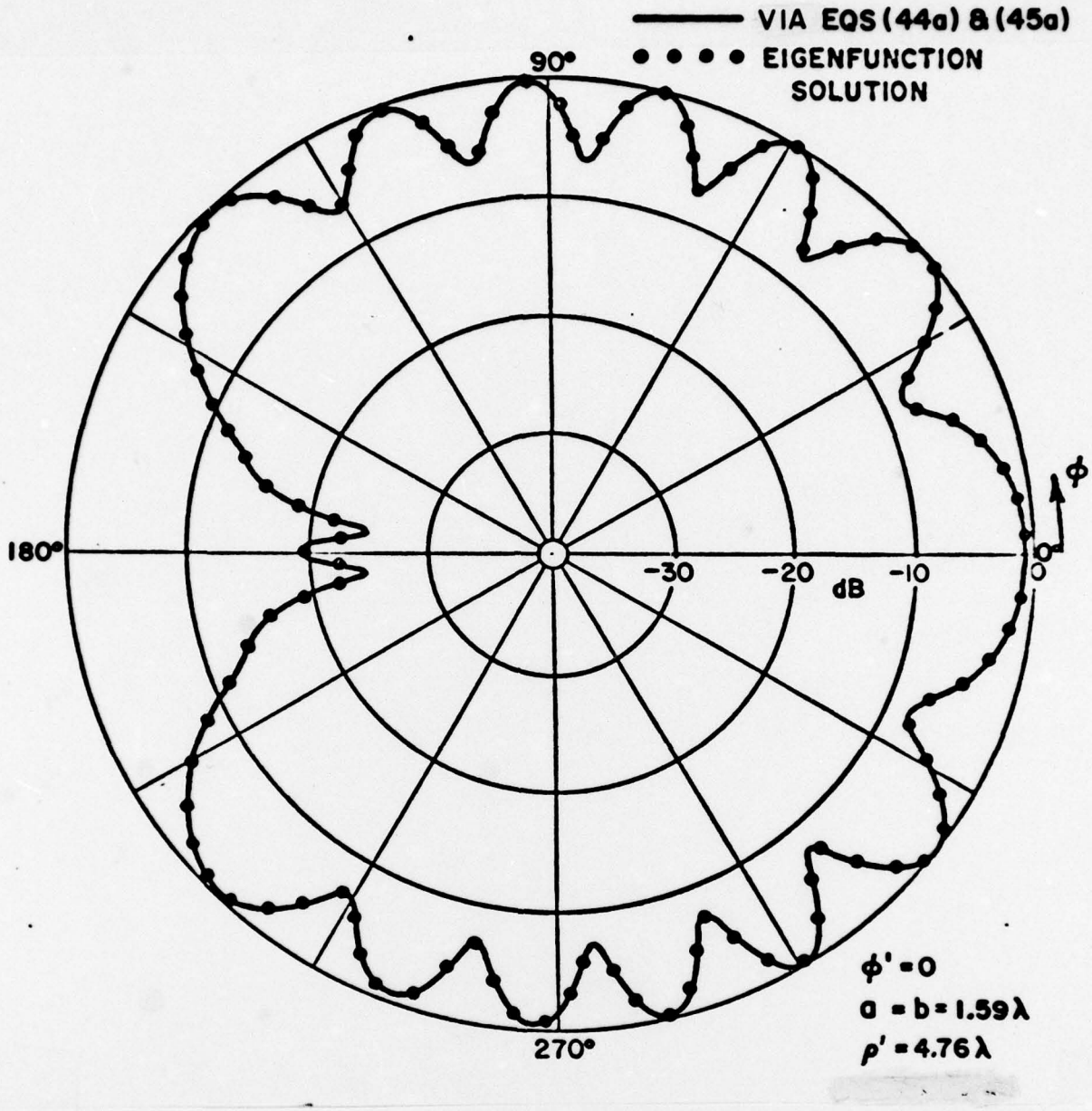

Figure 7b. Total field surrounding the cylinder of Figure 7a excited by an electric line source.

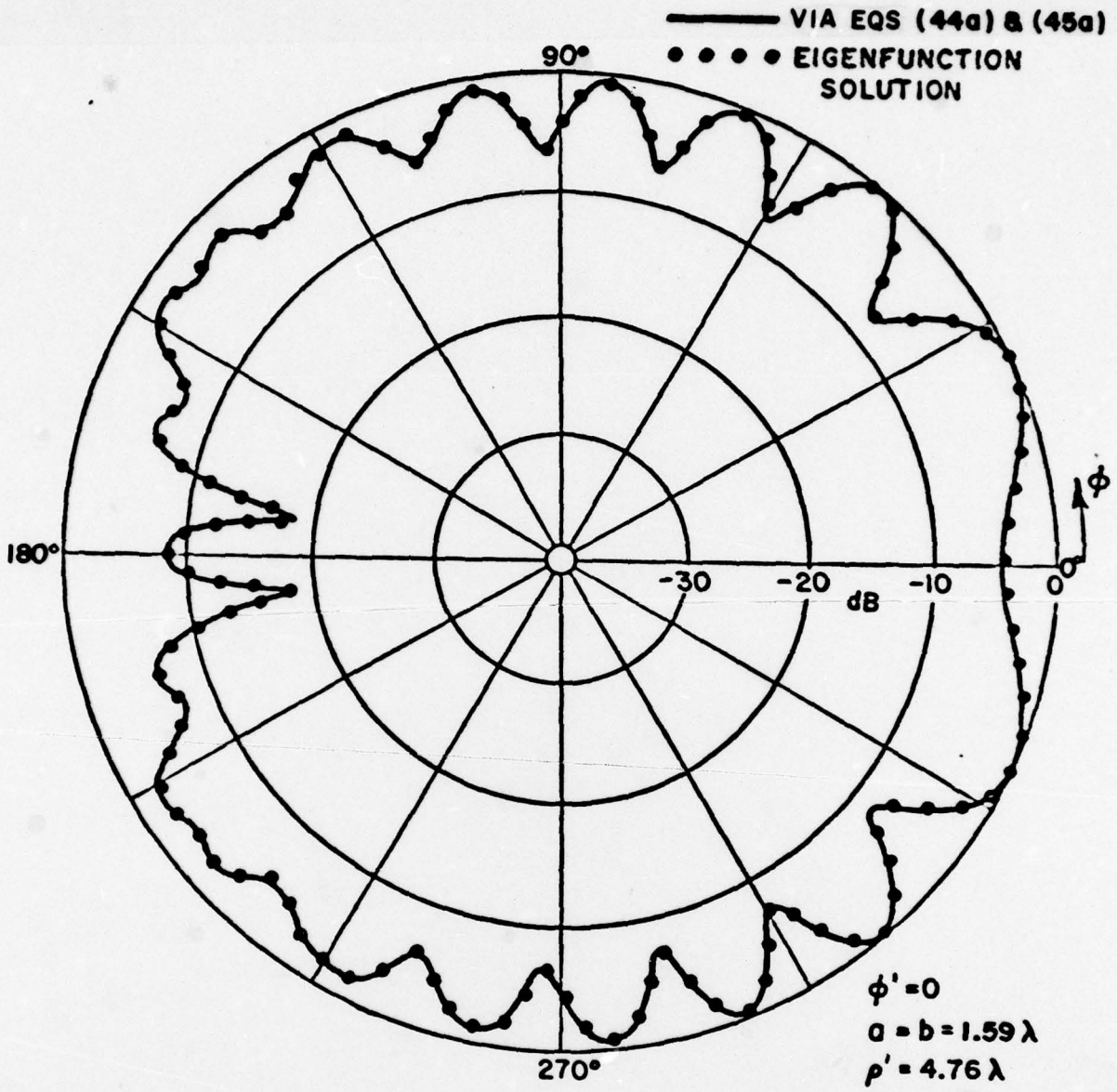

Figure 7c. Total field surrounding the cylinder of Figure 7a excited by a magnetic line source.

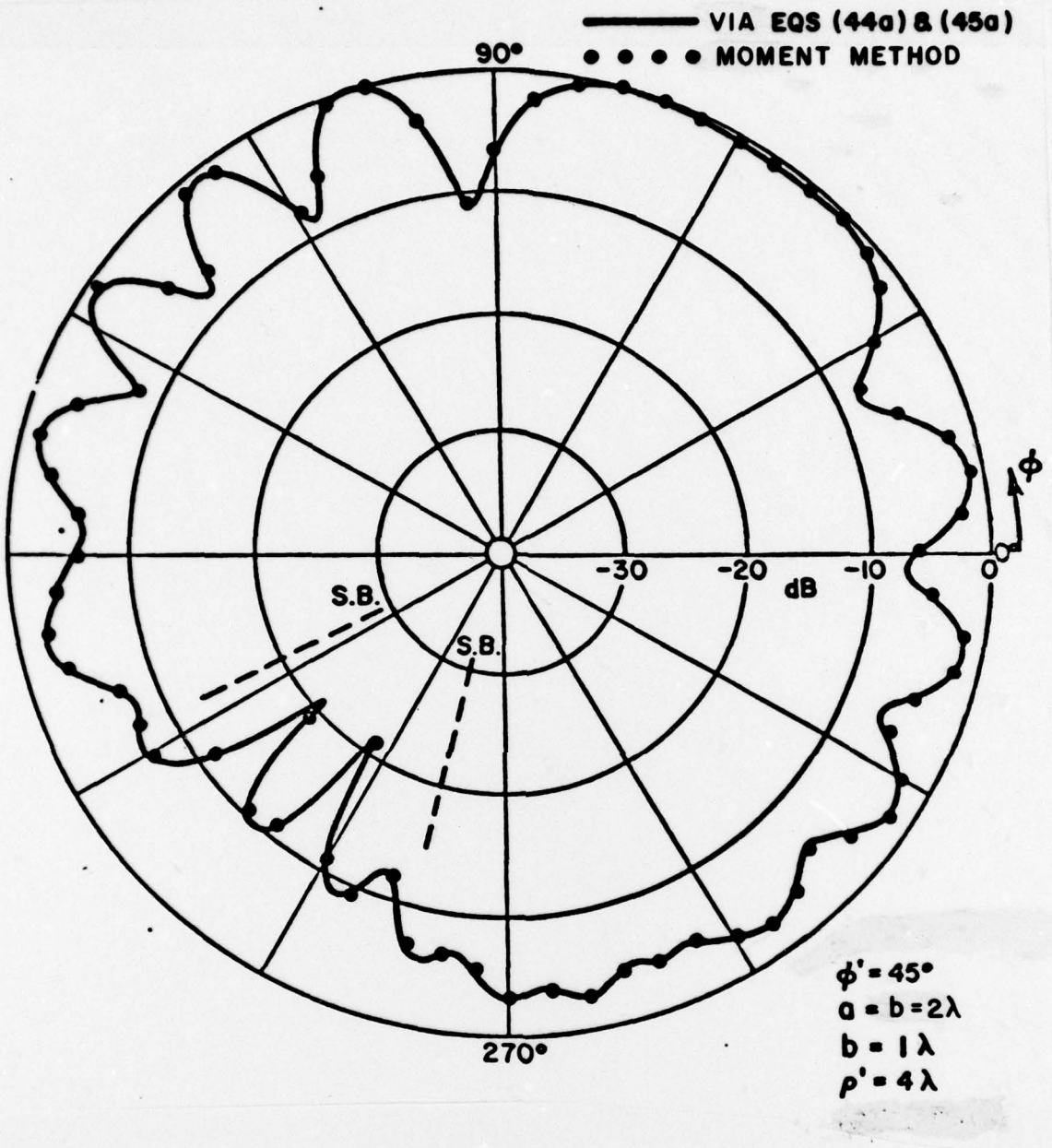

Figure 7d. Total far-field surrounding the cylinder of Figure 7a excited by a magnetic line source.

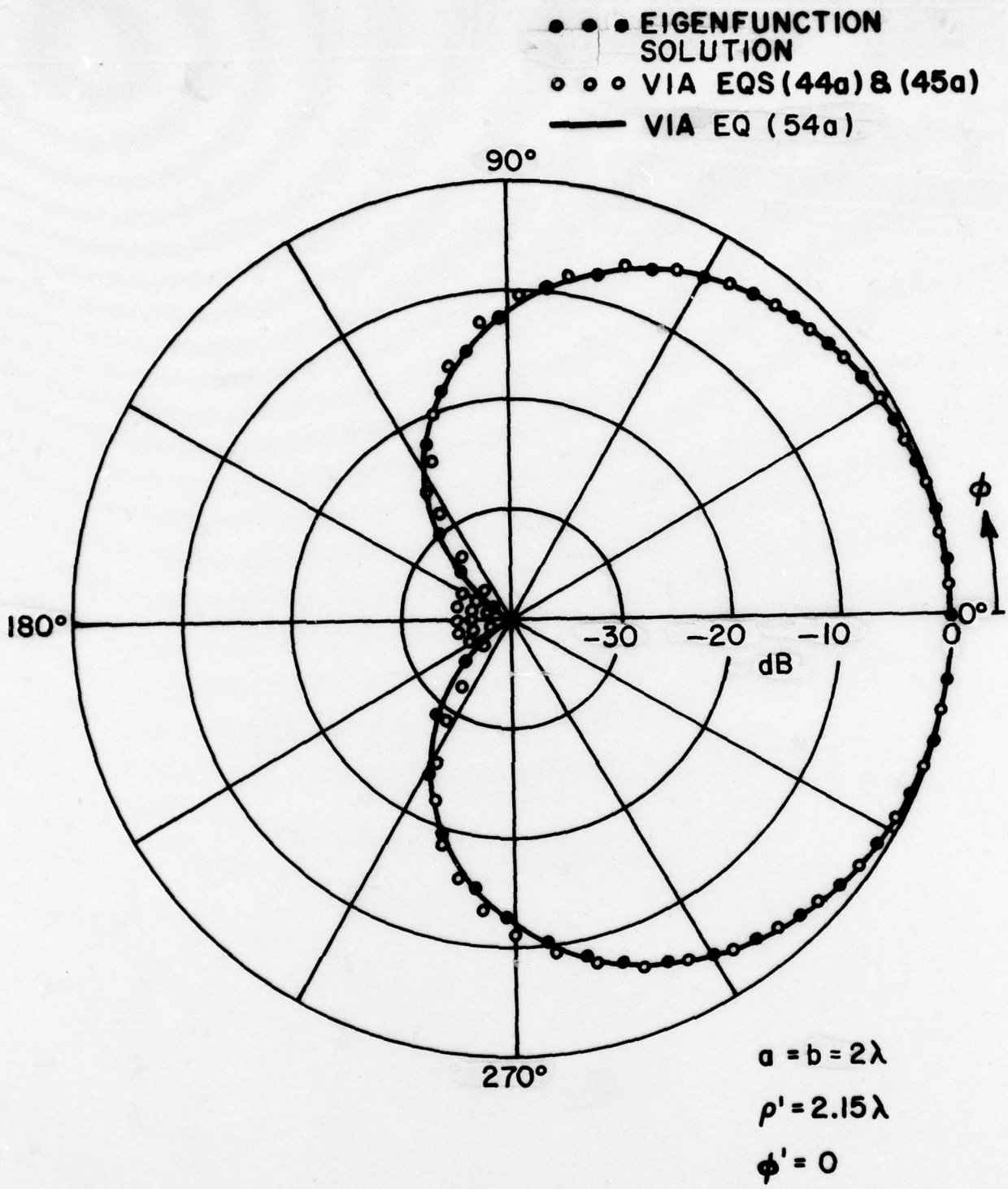

Figure 8a. Total field surrounding the cylinder of Figure 7a excited by an electric line source.

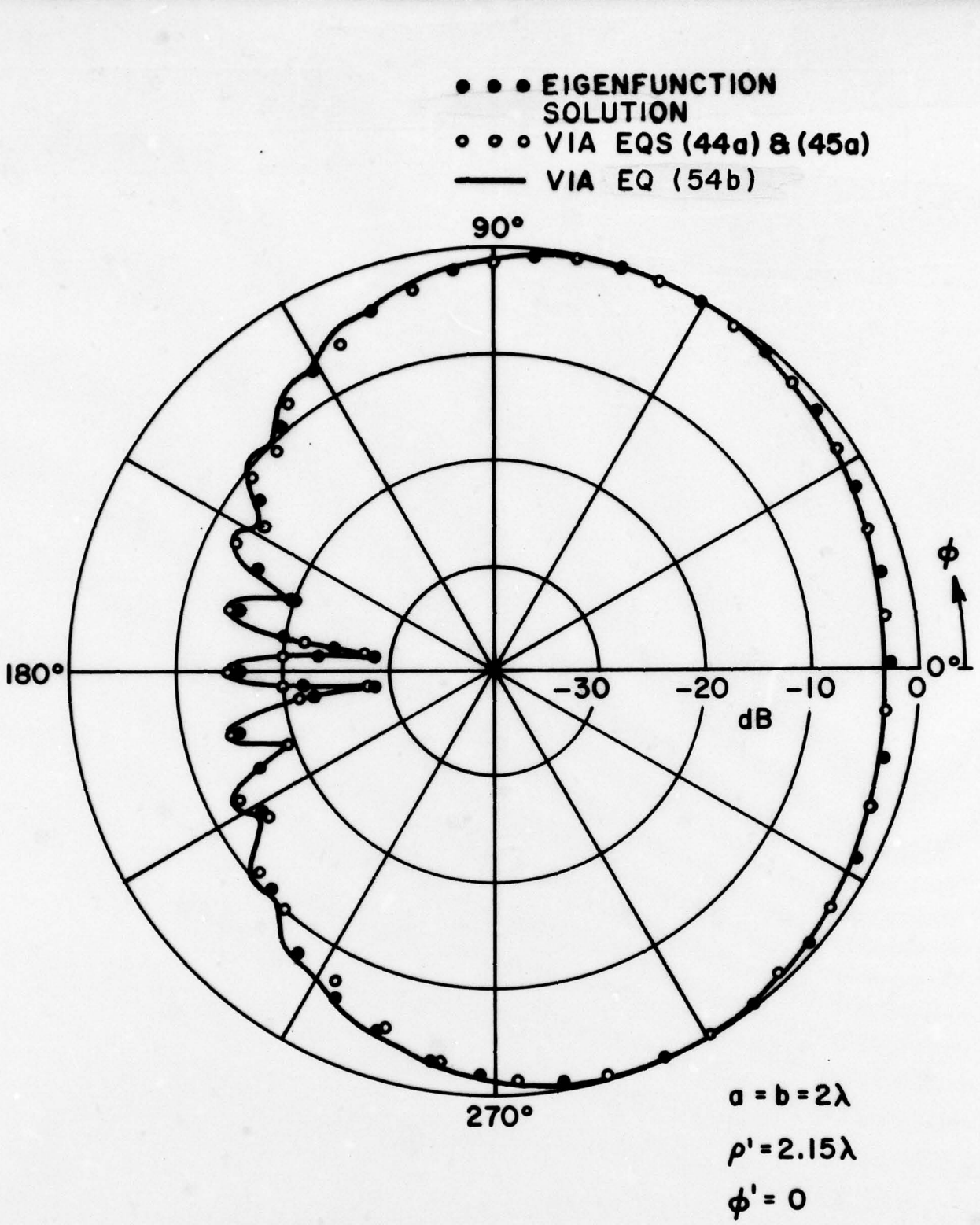

Figure 8b. Total field surrounding the cylinder of Figure 7a excited by a magnetic line source.

Incorporating (56a) and (56b) into (44a) and (45a) yields exactly the same limit value as the field point approaches the shadow boundary from either the shadow or the lit side; this limit value is

$$u(P)\Big|_{SB} \sim \frac{1}{2}\, u^{i}(P) - m(Q_1)\sqrt{\frac{2}{k}}\, e^{-j\frac{\pi}{4}} \begin{Bmatrix} p^*(o) \\ q^*(o) \end{Bmatrix} \frac{e^{-jk\ell_{SB}}}{\sqrt{\ell_{SB}}} \quad ; \quad \begin{cases} TE_z \text{ case} \\ TM_z \text{ case} \end{cases}$$

where ℓ_{SB} is the distance from Q_1 to P on the shadow boundary (SB). Thus, (44a) and (45a) yield a continuous total field at the shadow boundary. It can be shown for the circular cylindrical case that the total high frequency field based on (44a) and (45a) possesses derivatives along the normal direction to the shadow boundary which are also continuous to $O(1/\ell_{SB})$. In this connection, it has therefore been observed that the pattern in addition to being continuous is also relatively smooth. These observations hold also for the smooth convex cylinder case provided the local radius of curvature of the convex cylinder is slowly varying as assumed previously. The result of (53a) and (53b) is continuous across the shadow boundary as may be easily verified by inspection.

While the uniform result of (44a) and (45a) pertains to a perfectly conducting smooth, convex cylinder, a similar result can be obtained for a cylinder with an impedance boundary condition. However, the latter case has not been included here since the $\hat{P}_{s,h}$ functions which are now dependent on the non-zero value of the impedance, are not extensively tabulated.

Further extensions of the uniform result of (44a) and (45a) to treat the general three dimensional problem of the scattering of an arbitrary electromagnetic ray field by an arbitrary, smooth, perfectly conducting, convex surface will be presented in a future paper [Pathak, et. al.].

ACKNOWLEDGMENT

The author would like to express his sincere appreciation to Dr. W. D. Burnside and Dr. R. J. Marhefka, for their assistance in numerical calculations, and for their continued interest in this work.

REFERENCES

V. A. Borovikov and B. Y. Kinber (1974), Proc. IEEE, Vol. 62, No. 11, pp. 1416-1437.

J. J. Bowman, T. B. A. Senior, and P. L. E. Uslenghi (1969), Electromagnetic and Acoustic Scattering by Simple Shapes, North Holland Publishing Co., Amsterdam.

W. D. Burnside (1972), "Analysis of On-Aircraft Antenna Patterns," Report 3390-1, The Ohio State University ElectroScience Laboratory, Department of Electrical Engineering; prepared under Contract N62269-72-C-0354 for Naval Air Development Center.

W. D. Burnside, M. C. Gilreath, R. J. Marhefka, and C. L. Yu (1975), "A Study of KC-135 Aircraft Antenna Pattern," IEEE Trans. AP-5, pp. 309-316.

V. A. Fock (1946), "The Field of a Plane Wave Near the Surface of a Conducting Body," Izvestia Akademii Nauk (ser. Fiz.), Vol. 10, p. 171 (also in [Fock (1957)].

V. A. Fock (1951), "Fresnel Diffraction from Convex Bodies," Uspekii Fizicheskikh Nauk., Vol. 43, pp. 587-599. (Also in [Fock(1957)].

V. A. Fock (1957), "Diffraction, Refraction and Reflection Waves: Thirteen Papers," Air Force Cambridge Research Center Report AFCRC-TN-57-102, (AD 117276). Also V. A. Fock, Electromagnetic Diffraction and Propagation Problems, Pergamon Press, 1965.

V. I. Ivanov (1971), U.S.S.R. Journal of Computational Math. and Math. Phys. (Translated from Zl. Vychisl. Mat. Mat. Fiz.), Vol. 2, p. 216.

J. B. Keller (1953), "Proceedings of Symposium on Microwave Optics," Part II, McGill University, pp. 207-210. (AD 211500)

J. B. Keller (1956), "Diffraction by a Convex Cylinder," Trans. I.R.E., Vol. AP-24, pp. 312-321.

J. B. Keller (1962), "Geometrical Theory of Diffraction," J. Opt. Soc. Am., Vol. 52, No. 2, pp. 116-130.

R. G. Kouyoumjian and P. H. Pathak (1974), Proc. IEEE, Vol. 62, pp. 1448-1461.

N. A. Logan (1959), "General Research in Diffraction Theory," Vol. I, LMSD-288087; and Vol. II, LMSD-288088, Missiles and Space Division, Lockheed Aircraft Corp.

J. R. Wait and A. M. Conda (1959), "Diffraction of Electromagnetic Waves by Smooth Obstacles," Jour. of Res., N.B.S., Vol. 63D, No. 2, pp. 181-197.

N. A. Logan and K. S. Yee (1962), Electromagnetic Waves, Edited by R. E. Langer, Univ. of Wisconsin Press.

P. H. Pathak and R. G. Kouyoumjian (1974), Proc. IEEE, Vol. 62, pp. 1438-1447.

P. H. Pathak, W. D. Burnside and R. J. Marhefka, "An Asymptotic Result for the Scattering of Electromagnetic Waves by a Smooth Convex Surface," Report 4583-4, The Ohio State University ElectroScience Laboratory, Department of Electrical Engineering; prepared under Contract N62269-76-C-0554 for the Department of the Navy, (in preparation).